Biosensors and Bioelectronics 100 (2018) 23–27

Contents lists available at ScienceDirect

Biosensors and Bioelectronics

journal homepage: www.elsevier.com/locate/bios

Hybrid localized surface plasmon resonance and quartz crystal microbalance sensor for label free biosensing

Danni Hao*, Chunxiao Hu, James Grant, Andrew Glidle, David R.S. Cumming

School of Engineering, Rankine Building, University of Glasgow, Glasgow G12 8LT, UK

ARTICLE INFO

Keywords:
LSPR
QCM
Point-of-care

ABSTRACT

We report on the design and fabrication of a hybrid sensor that integrates transmission-mode localized surface plasmonic resonance (LSPR) into a quartz crystal microbalance (QCM) for studying biochemical surface reactions. The coupling of LSPR nanostructures and a QCM allows optical spectra and QCM resonant frequency shifts to be recorded simultaneously and analyzed in real time for a given surface adsorption process. This integration simplifies the conventional combination of SPR and QCM and has the potential to be miniaturized for application in point-of-care (POC) diagnostics. The influence of antibody-antigen recognition effect on both the QCM and LSPR has been analyzed and discussed.

1. Introduction

Optical and mechanically oscillating sensing techniques have applications in in-situ, label free sensing and analysis of chemical and biological binding reactions (Mayer and Hafner, 2011; Arnau, 2008). Optical sensing techniques, such as surface plasmonic resonance (SPR), typically measure the change in the refractive index arising from the molecular adsorption on the metal surface thus measures the molecular mass of thin films (Zong et al., 2008). Quartz crystal microbalance (QCM) devices use the resonance phenomenon of piezoelectric quartz where the frequency of its mechanical oscillation is dependent upon the acoustic mass of the sum of the deposited molecules and the solvent coupled to the adsorbed molecules. Therefore, in a surface adsorption process, the integration of optical and acoustic sensing can not only give information regarding weight but also the film hydration which provides insights into the conformational properties of the molecules in the formed layer and the biomolecule adsorption characteristics.

Owning to the complementary characteristics of SPR and QCM, methods of combining SPR and QCM devices have attracted significant interest. Studies have taken advantage of both modalities to evaluate the thickness of polymer films (Lee et al., 2007) and biomolecule adsorption (Zhou et al., 2004; Malmström et al., 2007). However, the optical and acoustic responses are measured sequentially on different devices, not at the same time on the same film. To eliminate the variations of the experimental conditions, a sensor that can record both the optical and acoustic signal simultaneously is essential. A hybrid sensor using a continuous thin film gold electrode on one side of a bulk-mode acoustic wave (BAW) sensor has been reported (Shinbo et al., 2012). SPR detection was performed by monitoring the variation in the angle of the reflected light from the electrode (Shinbo et al., 2012; Kim et al., 2010; Zong et al., 2008; Laschitsch et al., 2000). In this way it was possible to determine the adsorbed mass. Localized surface plasmon resonance (LSPR) has the advantage that measurements are made by collecting spectra, and suitable equipment is widely available. The sensitivity of LSPR is comparable to SPR in biomolecule binding reactions.(Willets and Van Duyne, 2007) Both LSPR sensor and QCM have great potential regarding to point-of-care (POC) tests. (Aćimović et al., 2014; Yuan and Han, 2015) Hence, in this paper, we report the design of a hybrid sensor that integrates transmission-mode LSPR with a QCM which can be useful for the analysis of immunological reactions, film structures and other biological sorption reactions.

2. Experimental

2.1. Materials

All chemicals were of analytical-reagent grade. Glycerine, (3-Aminopropyl) triethoxysilane (APTES), N-(3-Dimethylaminopropyl)-N′-ethylcarbodiimide hydrochloride (EDC), NaOH, bovine serum albumin (BSA), HCl, phosphate buffered saline (PBS) tablets, ethanolamine, rabbit IgG, anti-rabbit IgG, succinic acid and methyl isobutyl ketone (MIBK) were obtained from Sigma-Aldrich. Sulfo-N-hydroxysuccinimide(Sulfo-NHS) was obtained from Abcam. MICROPOSIT MF-CD26 developer was obtained from MicroChem. Isopropyl alcohol (IPA) was obtained from Fisher Scientific. NaOH and

* Corresponding author.
E-mail addresses: d.hao.1@research.gla.ac.uk (D. Hao), david.cumming.2@glasgow.ac.uk (D.R.S. Cumming).

http://dx.doi.org/10.1016/j.bios.2017.08.038
Received 6 July 2017; Received in revised form 14 August 2017; Accepted 16 August 2017

HCl stock solution was used to adjust the pH value of the buffer solution.

2.2. Equipment

The transmission spectra were obtained using a Foster and Freeman ffTA microspectrometer. The objective has a numerical aperture of 0.1 and magnification of 4 ×. The microspectrometer measurement area is 12.5 μm in diameter. Unpolarized light from a halogen lamp was normally incident on to the backside of the QCM. The transmitted light passed through the spectrometer and was analyzed and recorded by the ffTA software. The characterization of a standard QCM chip and a modified QCM chip was done using an Agilent vector network analyzer (VNA) E5071B. WinCal software was used to collect the return loss S11 spectra. An overview of the combined QCM and LSPR instrument setup can be found in the supplementary material Fig. S1. In addition to the hybrid QCM chip, a second reference QCM was mounted onto the same printed circuit board (PCB). The PCB used in the experiment was made in-house. The oscilloscope used in the experiment was a Tektronix TDS2000C. The QCM resonance frequency was collected by LabVIEW signal express software. A polyethylene terephthalate flow cell was made in-house using a 3D printer. Silicone sealant was applied to seal the flow cell and minimize the mechanical stress in the crystal (Rabe et al., 2003). Finally a glass slide was positioned on top of the flow cell to seal it.

2.3. Procedures

2.3.1. QCM design

A schematic of the hybrid SPR and QCM sensor is shown in Fig. 1. In contrast to traditional QCM devices that have continuous metallic films on both sides of the piezoelectric material our device has a 400 μm diameter window defined in the back electrode and a 400 μm × 400 μm array of Au LSPR nanodiscs patterned in the center of the front electrode. The opening in the back metal electrode is necessary to allow visible light to pass through the device. AT-cut quartz crystal wafers with a diameter of 13.6 mm and a fundamental resonant frequency of-5 MHz were purchased from ICM CO, INC. The LSPR nanostructures and QCM electrodes were fabricated on the quartz substrates using electron beam lithography and photolithography respectively. Fig. 1 shows the experimental results comparing the QCM chip with continuous metallic electrodes and the hybrid LSPR and QCM device. The resonance frequency of the modified QCM device with LSPR structures on it shifts from 5.0058MHz to 5.0115 MHz due to the loss of the metal mass at the center of the electrode. The hybrid LSPR and QCM chip has excellent performance with a Q factor increased by 1×10^4 compared to the standard QCM which has a Q factor of 5.5×10^4.

2.3.2. LSPR design

The spectral transmission characteristics of the LSPR Au nanostructures were simulated using *Lumerical FDTD*. The 60 nm thick Au nanodisc was sandwiched between a semi-infinite SiO_2 substrate and a semi-infinite SiO_2 superstrate. The Au nanodisc was illuminated by a 400 nm to 1 μm plane-wave source, propagating in the z direction, and the transmission spectra were recorded by a frequency-domain field monitor. Symmetric boundary conditions were defined along the x and y axes and perfectly matched layers were set at the top and bottom boundaries to absorb any unwanted reflections. A mesh cell with size of $\Delta x = \Delta y = \Delta z = 5$ nm was set in the region encompassing the Au metal nanodisc layer and the SiO_2 surrounding it. In the simulations, Johnson and Christy's experimental values were used for the complex permittivity data of Au (Johnson and Christry, 1972).

A number of different Au nanostructures were simulated, fabricated and characterized on quartz substrates. Fig. 2 shows the scanning electron micrographs, simulation data and experimental results of several different designs. The resonance wavelength, λ_{peak}, which is the LSPR absorption peak, shows a red shift with increasing periodicity (a) while λ_{peak} blue-shifts as the diameter (d) of the Au nanodiscs decreases. The sensitivity, defined as $\Delta\lambda_{peak}$/RIU, of the LSPR sensor is greater at longer wavelengths. As shown in supplementary Fig. S2, plasmonic sensors with resonances at longer wavelengths display greater sensitivity than those with resonances in the blue region (Willets and Van Duyne, 2007). We tailored the design such that λ_{peak} was in the 800–900 nm (a = 450 nm, d = 200 nm) range as the spectra shows a higher absorption intensity (transmission minimum), and it is close to the upper limit of our spectrometer measurement range.

2.3.3. Fabrication of the integrated chip

The hybrid LSPR and QCM device was fabricated on a 330 μm quartz substrate as follows. First, a 300 nm thick bi-layer of poly(-methyl methacrylate) (PMMA) was spin coated on to the quartz surface. The resist was then baked on a hot-plate at 156 °C for 5 min per coating. To avoid charging effects that can damage the substrate when carrying out electron beam lithography (EBL), a 30 nm Al layer was evaporated on top of the resist. Patterns were written by EBL at a beam voltage of 100 kV. The Al charge dissipation layer was removed by MF-CD26 and the PMMA resist developed in a solution of MIBK: IPA (1:2). Finally, a 3 nm/60 nm Ti/Au layer was evaporated on to the sample (Ti used as an adhesion layer) and the sample then immersed in a beaker of hot acetone for 2 h for lift-off of the unwanted metal. The

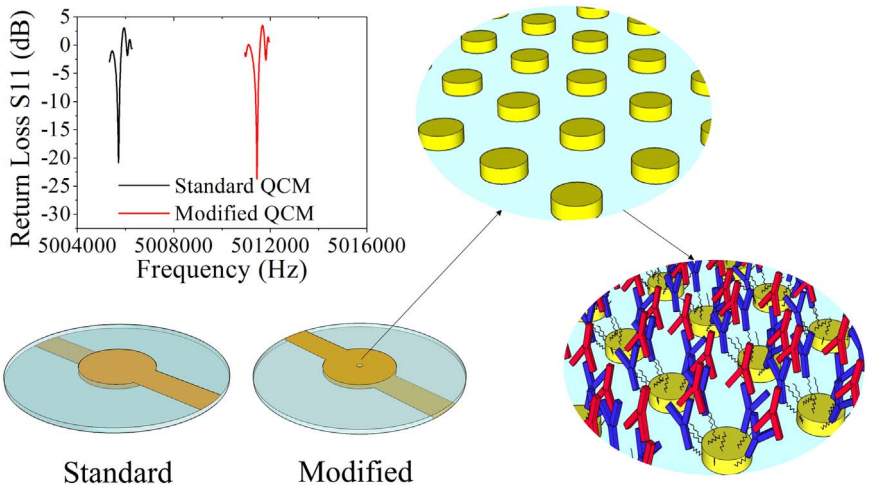

Fig. 1. VNA measured return loss (S11) spectra of the standard QCM and hybrid LSPR and QCM. inset: schematic of the modified QCM showing the antibody/antigen binding reaction attached to the Au LSPR nanostructures.

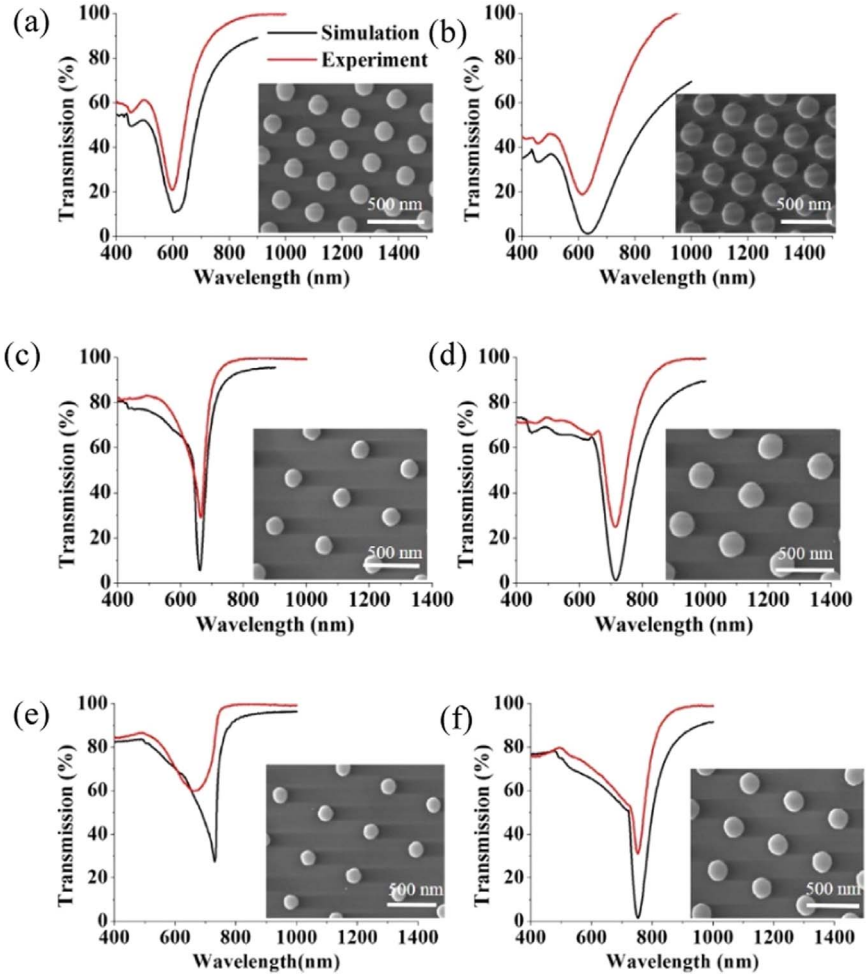

Fig. 2. Simulated and experimental transmission spectra and scanning electron micrographs of Au nanodisc arrays for selected periodicities and nanodisc diameters. *a* and *b* are the periodicity and disc diameter, respectively. (a) *a* = 300 nm, *b* = 150 nm (b) *a* = 300 nm, *b* = 200 nm (c) *a* = 450 nm, *b* = 150 nm (d) *a* = 450 nm, *b* = 200 nm (e) *a* = 500 nm, *b* = 150 nm (f) *a* = 500 nm, *b* = 200 nm.

QCM electrodes were formed by evaporating a 10 nm/100 nm Ti/Au layer on to both sides of the quartz substrate using a standard photolithography and lift-off process.

2.3.4. Characterization of the hybrid device

In order to verify that the hybrid device operated as expected, experiments were conducted using a glycerine- water solution. Both the LSPR wavelength and QCM frequency were recorded and the simulated, analytical and experimental results are shown in Fig. 3. Sauerbrey's theory was used to calculate the QCM frequency (Komplin and Pietro, 1995).

$$\Delta f = \sqrt{\frac{f_0^3}{\pi \mu_q \rho_q} \sqrt{\eta_l \rho_l}}$$

where f_0 is the base resonant frequency of the crystal, μ_q = 2.65 g/cm^3 and ρ_q = 2.95×10^{11} g/cm s^2 are the elastic modulus and density of quartz, respectively, and η_l and ρ_l are the viscosity and density of the liquid, respectively. The refractive indices and viscosity of differing concentrations of glycerine-water solution are given by Ref. (Hoyt, 1934) and Ref. (Segur and Oberstar, 1951).

The resonant transmission dip, λ_{peak}, is dependent upon the refractive index n_m at the Au–liquid interface and the shift of λ_{peak} has been described by the following relation (Haes and Van Duyne, 2002):

$$\Delta\lambda_{peak} = m(\Delta n_m)[1-\exp\left(\frac{-2d}{l_d}\right)]$$

Where m is the bulk refractive-index response of the nanoparticle(s); Δn is the change in refractive index induced by the adsorbate; d is the effective adsorbate layer thickness; and l_d is the characteristic electromagnetic field decay length which is sensitive to the shape of the nanoparticle. Our simulations and experiments agree with this relationship between the LSPR peak wavelength and the refractive index. The (1,0) resonance wavelength red-shifts with increasing refractive index of the solution. The sensitivity of the LSPR is 273 nm/RIU for the experimental result, which is comparable to the simulated value of 321 nm/RIU. The experimental resonant frequency of the hybrid QCM decreases with increasing glycerine concentration and shows excellent agreement with the analytical prediction.

2.3.5. Setup for the simultaneous recording

A measurement setup was constructed to monitor the LSPR and QCM signal simultaneously. The transmission spectra were measured using the aforementioned spectrometer. The interval between each spectral recording was set at 3 s; a trade-off between the signal-to-noise ratio and recording speed. The QCM frequency was obtained using a frequency comparison circuit (Bruckenstein and Shay, 1985) and the frequency difference between the working crystal and the reference crystal monitored by the oscilloscope. The computer simultaneously ran two pieces of recording software: ffTA software for the microspectrometer; and LabView to acquire the QCM data and to synchronize the data acquisition.

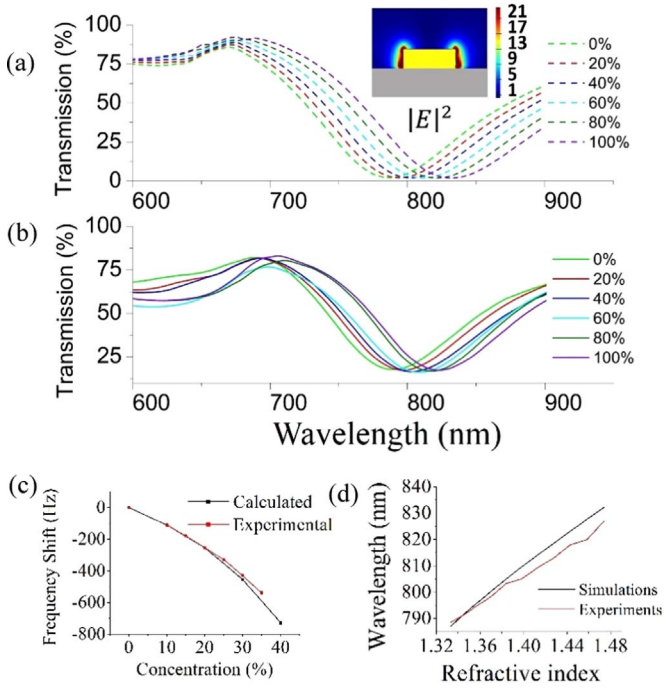

Fig. 3. (a) Simulated and (b) measured transmission spectra for the LSPR sensors in glycerine-water solutions of differing concentrations. Inset of (a): Electric field intensity distributions at the resonance wavelength. The yellow region represents the gold nanodisc and the grey region represents the SiO_2 substrate. (c) Frequency shift of the hybrid QCM versus increasing concentrations of glycerine-water solutions. (d) LSPR resonance wavelength shift as a function of change in the bulk refractive index.

2.3.6. Surface functionalization

Anti-IgG antibodies were covalently immobilized on the sensing surface as follows. First, a 30 s, 80 W oxygen plasma treatment was applied to the sensing surface of the hybrid LSPR and QCM device. Next, the chip was immersed in APTES for 7 h to create a self-assembled monolayer (SAM). After this step, the QCM frequency decrease is 14.4 Hz (averaged from three experiments), which agrees with previously published work (Oliver et al., 2011). The chip was subsequently rinsed with ethanol to remove the chemisorbed molecules. Next, Sulfo-NHS (10.6 mM), EDC-HCl (40.7 mM) and Succinic acid (400 mM) were mixed in phosphate buffer. After bringing the pH back to 7.2, the mixture was injected onto the sample surface in order to from the carboxylic acid group. Then, 10 µl aliquots of a solution of EDC-HCl (40.7 mM) and Sulfo-NHS (10.6 mM) in PBS buffer with a pH of 6 was deposited on the sample surface and left at room temperature for 2 h in order to activate the carboxylic acid group. After washing the flow cell with PBS buffer3, 1.5 mL of 100 µg/mL anti-rabbit IgG was then put into the cell and incubated at room temperature for 10 min for covalent immobilization. The cell was then rinsed using PBS and BSA was introduced for 15 min to block the surface against unspecific binding of the antibody. After another rinse with PBS, the recording was initialized for basal resonant frequency stabilization. The rabbit IgG solution (10–100 µg/mL) was injected into the cell at a flow rate of 0.18 mL/min and the LSPR transmission shift and the QCM frequency change continuously monitored. On completion of the experiment the chip surface was regenerated using a 10 min 150 W oxygen plasma treatment. The experiments for all concentrations have been repeated three times and averaged. The standard deviation for each concentration and each sensing techniques can be found in Fig S3.

3. Results and discussion

As seen in Fig. 4, after introducing IgG molecules into the flow cell, both the LSPR wavelength and QCM signal increase and correlation

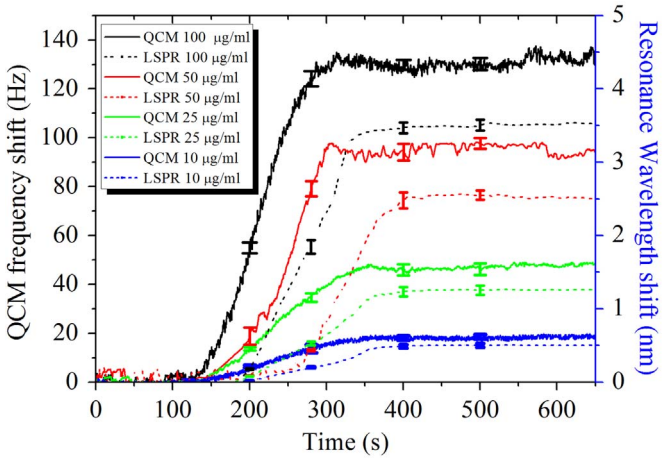

Fig. 4. Changes in QCM frequency (line) and LSPR resonance wavelength (dotted line and data points) versus time. Rabbit IgG was injected at t = 100 s.

can be made between the QCM frequency shift and the LSPR resonance wavelength shift (see Fig. S3). The linear range of the sensor is between 10–50 µg/mL and the limit of detection (LOD) is 5 µg/mL for QCM and 1.88 µg/mL for LSPR measurements (for more information please see supplementary material). The adsorbed mass measured by the QCM is 1593 ng cm^{-2} for 50 µg/mL IgG solution which is in agreement with published literature (He et al., 2012). The dissociation constant (K_D) describes the affinity between the antibody and its antigen. The data was plotted in Fig. S4 and fitted to the Hill equation (see supplementary material); the calculated dissociation constant of the reaction was 6.67 × 10^{-7} M.

We can also see from Fig. 4 that the QCM signal starts changing in the first few seconds after the introduction of the antigen while the LSPR response has a ~ 40 s delay. The LSPR signal change is slower than the QCM shift for two primary reasons. The analyte is introduced a distance of ~ 7 mm from where the LSPR structures reside. The analyte must diffuse to the Au nanodisc region and bind with the LSPR structures to illicit a change in the LSPR wavelength. In contrast the QCM measures the area-average result therefore it shows a response as soon as the binding action starts at the edge of the gold electrode. Secondly, as seen in the inset of Fig. 3(a), the electric field distribution suggests that LSPR-active region is mostly on the sidewall of the gold nanodiscs. The introduced antigen must bind to the antibodies residing on these sidewalls to obtain the full LSPR response.

4. Conclusions

We have demonstrated the simultaneous measurement capabilities of a hybrid sensor that integrates a transmission-mode LSPR sensor with a QCM sensor. The device provides a versatile tool for studying dynamic processes in biomolecular reactions and thin films. The measurement platform can be further improved to include a QCM dissipation measurement or choosing a QCM to operate at a higher frequency to obtain higher sensitivity. Moreover, the costly and bulky equipment required to detect the LSPR and QCM signal (spectrometer and VNA respectively) could be replaced by Si pn diodes and thin film bulk acoustic resonators resulting in a low-cost, portable, hybrid LSPR and QCM device suitable for POC diagnostics.

Acknowledgements

We acknowledge the technical staff of James Watt Nano-fabrication Center (JWNC) for assisting in the fabrication of samples. This work was supported by the Engineering and Physical Sciences Research Council (EPSRC) grant EP/K021966/1. The dataset for the results in the paper can be found at http://dx.doi.org/10.5525/gla.researchdata.447.

Appendix A. Supporting information

Supplementary data associated with this article can be found in the online version at doi:10.1016/j.bios.2017.08.038.

References

Aćimović, S.S., Ortega, M.A., Sanz, V., Berthelot, J., Garcia-Cordero, J.L., Renger, J., Maerkl, S.J., Kreuzer, M.P., Quidant, R., 2014. Nano Lett. 14, 2636–2641. http://dx.doi.org/10.1021/nl500574n.

Arnau, A., 2008. Sensors 8, 370–411. http://dx.doi.org/10.3390/s8010370.

Bruckenstein, S., Shay, M., 1985. Acta 30, 1295–1300. http://dx.doi.org/10.1016/0013-4686(85)85005-2.

Haes, A.J., Van Duyne, R.P., 2002. J. Am. Chem. Soc. 124, 10596–10604. http://dx.doi.org/10.1021/ja020393x.

He, J., Lu, Y., Fang, J., Ma, H., 2012. Sci. China Chem. 55, 175–181. http://dx.doi.org/10.1007/s11426-011-4467-8.

Hoyt, L.F., 1934. Ind. Eng. Chem. 26, 329–332. http://dx.doi.org/10.1021/ie50291a023.

Johnson, P.B., Christry, R.W., 1972. Phys. Rev. B 6, 4370–4379. http://dx.doi.org/10.1103/PhysRevB.6.4370.

Kim, J., Kim, S., Ohashi, T., Muramatsu, H., Chang, S.M., Kim, W.S., 2010. Bioprocess Biosyst. Eng. 33, 39–45. http://dx.doi.org/10.1007/s00449-009-0370-5.

Komplin, G.C., Pietro, W.J., 1995. Rev. Sci. Instrum. 66, 1131–1135. http://dx.doi.org/10.1063/1.1145992.

Laschitsch, A., Menges, B., Johannsmann, D., 2000. Appl. Phys. Lett. 77, 2252–2254. http://dx.doi.org/10.1063/1.1315338.

Lee, B.S., Chi, Y.S., Lee, K.B., Kim, Y.G., Choi, I.S., 2007. Biomacromolecules 8, 3922–3929. http://dx.doi.org/10.1021/bm7009043.

Malmström, J., Agheli, H., Kingshott, P., Sutherland, D.S., 2007. Langmuir 23, 9760–9768. http://dx.doi.org/10.1021/la701233y.

Mayer, K.M., Hafner, J.H., 2011. Chem. Rev. 111, 3828–3857. http://dx.doi.org/10.1021/cr100313v.

Oliver, M.J., Hernando-García, J., Pobedinskas, P., Haenen, K., Ríos, A., Sánchez-Rojas, J.L., 2011. Colloids Surf. B Biointerfaces 88, 191–195. http://dx.doi.org/10.1016/j.colsurfb.2011.06.030.

Rabe, J., Büttgenbach, S., Schröder, J., Hauptmann, P., 2003. IEEE Sens. J. 3, 361–368. http://dx.doi.org/10.1109/JSEN.2003.815783.

Segur, J.B., Oberstar, H.E., 1951. Ind. Eng. Chem. 43, 2117–2120. http://dx.doi.org/10.1021/ie50501a040.

Shinbo, K., Ishikawa, H., Baba, A., Ohdaira, Y., Kato, K., Kaneko, F., 2012. Appl. Phys. Express 5, 36603. http://dx.doi.org/10.1143/APEX.5.036603.

Willets, K.A., Van Duyne, R.P., 2007. Annu. Rev. Phys. Chem. 58, 267–297. http://dx.doi.org/10.1146/annurev.physchem.58.032806.104607.

Yuan, Y.J., Han, K., 2015. 2015 IEEE Sens. Proc. 16, 8731–8735. http://dx.doi.org/10.1109/ICSENS.2015.7370589.

Zhou, C., Friedt, J., Angelova, A., Choi, K., Laureyn, W., Frederix, F., Francis, L.A., Campitelli, A., Engelborghs, Y., Borghs, G., 2004. Langmuir 20, 5870–5878. http://dx.doi.org/10.1021/la036251d.

Zong, Y., Xu, F., Su, X., Knoll, W., 2008a. Anal. Chem. 80, 5246–5250. http://dx.doi.org/10.1021/ac800393d.